**(b)**

| Peak No. | $(M+H)^+$ Observed | $(M+H)^+$ Calculated | Assignment |
|---|---|---|---|
| 1 | 830.6<br>873.5<br>1072.6 | 830.4<br>873.4<br>1072.5 | QGVAEAAGK (24-32)<br>EGVVAAAEK (13-21)<br>AKEGVVAAAEK (11-21) |
| 2 | 1180.7<br>1295.8<br>1524.8 | 1180.6<br>1295.6<br>1524.8 | TKEGVLYVGSK (33-43)<br>EGVVHGVATVAEK (46-58)<br>TKEGVVHGVATVAEK (44-58) |
| 3 | 951.5 | 951.5 | EGVLYVGSK (35-43) |
| 4 | 1295.7 | 1295.6 | EGVVHGVATVAEK (46-58) |
| 5 | 770.5 | 770.3 | MDVFMK (1-6) |
| 6 | 1606.6 | 1606.8 | TVEGAGSIAAATGFVKK (81-97) |
| 7 | 2157.2 | 2157.1 | TKEQVTNVGGAVVTGVTAVAQK (58-80) |
| 8 | 1478.5 | 1478.7 | TVEGAGSIAAATGFVK (81-96) |
| 9 | 1928.0 | 1928.0 | EQVTNVGGAVVTGVTAVAQK (61-80) |
| 10 | 4295.0 | 4286.7 | NEEGAPQEGILEDMPVDPDNAYEMPSEEGYQDYEPEA (103-140) |
| 11 | 803.0 | 802.3.0 | M*DVFM*K (1-6) (M*:methionine sulfoxide) |
| 12 | 4322.0 | 4318.7 | NEEGAPQEGILEDM*PVDPDNAYEM*PSEEGYQDYEPEA (103-140) |
| 13 | 4311.0 | 4302.7 | NEEGAPQEGILEDM#PVDPDNAYEM#PSEEGYQDYEPEA (103-140)<br>(One of two methionine residues (M#) was oxidized) |
| 14 | 4312.0 | 4302.7 | NEEGAPQEGILEDM#PVDPDNAYEM#PSEEGYQDYEPEA (103-140) |
| 15 | 802.0 | 802.3 | M*DVFM*K (1-6) |
| 16 | 4322.0 | 4318.7 | NEEGAPQEGILEDM*PVDPDNAYEM*PSEEGYQDYEPEA (103-140) |
| 17 | 4311.0 | 4302.7 | NEEGAPQEGILEDM#PVDPDNAYEM#PSEEGYQDYEPEA (103-140) |
| 18 | 4312.0 | 4302.7 | NEEGAPQEGILEDM#PVDPDNAYEM#PSEEGYQDYEPEA (103-140) |
| 19 | 803.0 | 802.3 | M*DVFM*K (1-6) |
| 20 | 4322.0 | 4318.7 | NEEGAPQEGILEDM*PVDPDNAYEM*PSEEGYQDYEPEA (103-140) |

**Fig. 3** *(legend on previous page)*

to Met5, Met116, Met127, and their neighboring residues (Fig 6a). The observed chemical shift differences are mostly attributable to the oxidation of methionine residues. The differences in peak intensities between Exi-monomer and control monomer were also generally small (Fig. 6c). These results indicate that the dynamical features of both synuclein monomers are almost the same, and methionine oxidation itself does not greatly influence the structural characteristics of α-synuclein.

It is noteworthy that significant reductions in signal intensity [$I$(Exi-dimer)/$I$(control monomer)< 0.8] were observed for the peaks originating from the N-terminal region (1–60) of Exi-dimer compared with the control monomer (Fig. 6d). This result shows that the N-terminal regions are involved in exifone-induced dimerization of α-synuclein, in accordance with the results obtained from Asp-N digestion of the Exi-dimer. The gradual reduction in the signal intensities might be explained by heterogeneous dimerization around the N-terminus. The observed reduction in signal intensity, in our case, was not due to chemical exchange between the inhibitor-free and inhibitor-bound states of α-synuclein, as had been suggested by Rao *et al.*,[10] because the inhibitor-induced dimer and monomer were each purified to homogeneity and free or exchangeable inhibitors were removed by gel-filtration column chromatography and buffer exchange. Similar NMR spectra were observed for dopamine- and gossypetin-induced dimers (Supplementary Fig. S4), indicating that the N-terminal dimerization modes induced by dopamine, exifone, and gossypetin are the same or at least very similar. On the other hand, the C-terminal portion of exifone-bound dimer was still predominantly random coil in character, as observed in the control monomeric α-synuclein. These

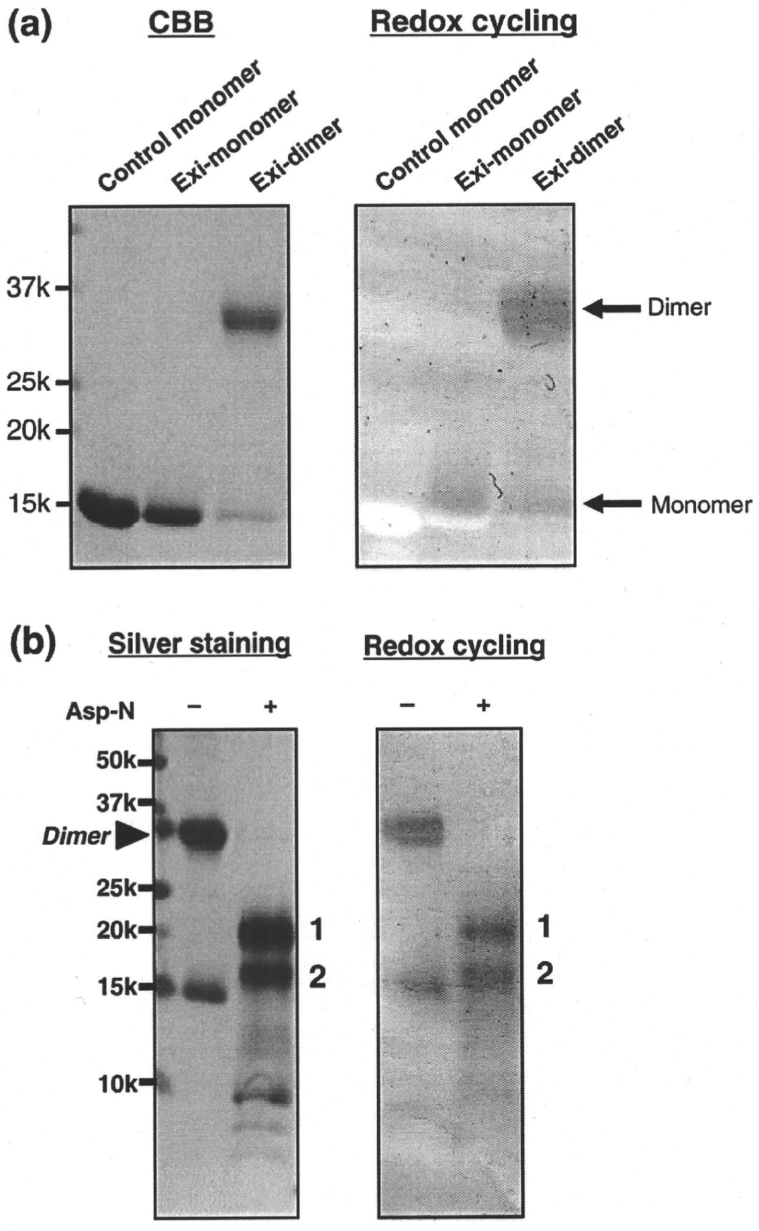


**Fig. 4.** Detection of exifone bound to α-synucleins by redox-cycling staining. (a) Control monomer, Exi-monomer, and Exi-dimer were stained with Coomassie brilliant blue (left) or by redox cycling (right). Exifone-bound α-synucleins were stained by redox cycling, appearing as purple-blue bands in the Exi-monomer and Exi-dimer lanes, due to NBT reduction to formazan (right). (b) Asp-N digestion of Exi-dimer. Exi-dimer was digested with endoproteinase Asp-N and the fragments were detected by silver staining (left) and redox staining (right). Two major bands corresponding to 20 kDa and 16 kDa (nos. 1 and 2, respectively) were positive for redox-cycling staining.

observations indicate the importance of the N-terminal region in α-synuclein assembly.

It is of note that three missense mutations in familial PD (A30P, E46K, and A53T) are located in the N-terminal region of α-synuclein. Recent NMR analyses suggest that these mutations may be altering the physicochemical properties of the protein, such as net charge (E46K) and secondary-structure propensity (A30P and A53T).[19] The binding of exifone, gossypetin, or dopamine to α-synuclein might also alter the net charge and/or secondary-structure propensity.

We did not observe the colloidal formation of exifone, gossypetin, or dopamine by electron microscopy (data not shown) as reported by Feng *et al.*[5] The discrepancy might be due to differences in the compounds used or differences in the proteins investigated. The inhibition mechanism of these three compounds seems rather specific because the N-terminal region was specifically involved in inhibitor binding, which is in contrast to the nonspecific colloidal inhibition.

In summary, we have characterized the inhibitor-bound α-synuclein dimer and showed that the N-terminal region (1–60) plays a key role in dimerization and inhibitor binding. Further studies are under way in our laboratory to elucidate the mechanisms of inhibitor-induced oligomer formation at atomic resolution.

## Materials and Methods

### Antibodies

Polyclonal antibodies were raised against synthetic peptides corresponding to residues 1–10, 11–20, 21–30, 31–40, 41–50, 51–60, 61–70, 75–91, and 131–140 of human α-synucleins, prepared as described previously.[12] Antibody

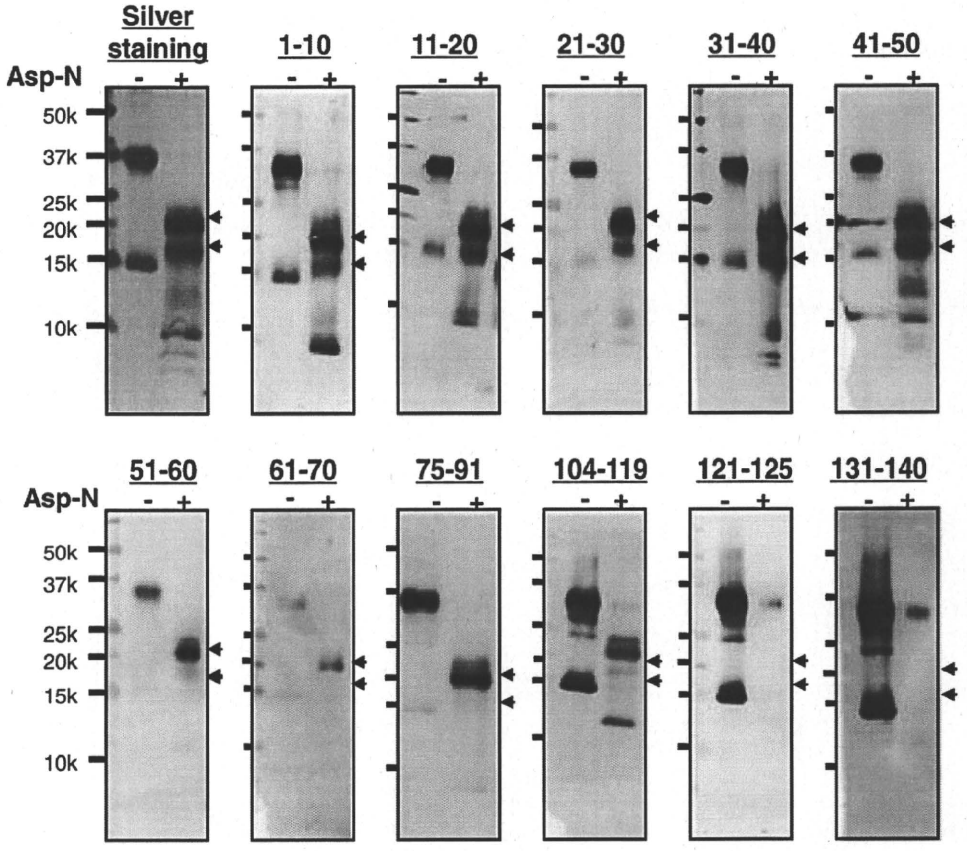


**Fig. 5.** Immunoblot analysis of Asp-N digests of Exi-dimer. Silver staining and immunoblots of Asp-N digests of Exi-dimer with a panel of anti-α-synuclein antibodies raised against nine peptides (corresponding to residues 1–10, 11–20, 21–30, 31–40, 41–50, 51–60, 61–70, 75–91, and 131–140).[12] Experimental details are given in Materials and Methods. Two major fragments (band nos. 1 and 2) were detected with silver staining (indicated with arrowheads). Fragment no. 1 was positive for antibodies to the N-terminal region, 1–97, and no. 2 was positive for antibodies to the N-terminal region, 1–50.

Syn259, which recognizes residues 104–119 of α-synuclein, was kindly provided by Dr. S. Nakajo. Monoclonal antibody Syn211, which recognizes residues 121–125 of α-synuclein, was purchased from Zymed.

### Protein expression and purification

Expression of isotopically labeled α-synuclein was performed as described.[13] Human α-synuclein cDNA in bacterial expression plasmid pRK172 was used for production of isotopically labeled protein for NMR analyses.[20] Codon 136 was changed from TAC to TAT by site-directed mutagenesis to avoid cysteine misincorporation.[21] Uniformly $^{15}$N-labeled α-synuclein was expressed in *Escherichia coli* BL21(DE3) cells grown in M9 minimal medium containing 1 g/L [$^{15}$N]$NH_4Cl$, while unlabeled α-synuclein was expressed using LB medium. Cell lysates were subjected to boiling and subsequently to ammonium sulfate precipitation. The precipitated α-synuclein was extensively dialyzed against 20 mM Tris–HCl (pH 8.0) and then purified with DEAE ion-exchange chromatography.

### Preparation of inhibitor-bound α-synuclein monomers and dimers

Purified $^{15}$N-labeled recombinant α-synuclein (9 mg/mL) was incubated with 2 mM inhibitor (exifone, gossypetin, or dopamine; see Fig. 1) for 30 days at 37 °C in 30 mM Tris–HCl containing 0.1% sodium azide. The samples were then centrifuged at 113,000*g* for 20 min. The supernatants were loaded on a Sephadex G-25 gel-filtration column to separate oligomers from unbound inhibitor. The eluates were fractionated on a Superdex 200 gel-filtration column (1 cm×30 cm), eluted with 10 mM Tris–HCl (pH 7.5) containing 150 mM NaCl. Eluates were monitored at 215 nm. α-Synuclein monomer and dimer fractions were each concentrated and the concentrates were subjected to NMR analysis. Protein concentrations were determined using HPLC and bicinchoninic acid protein assay kit (Pierce).

### Mass spectrometry

Samples were spotted on a sample plate and mixed with the matrix solutions, saturated sinapic acid (Fluka) or α-cyano-4-hydroxycinnamic acid (Fluka) in 50% acetonitrile/$H_2O$ containing 0.1% (v/v) trifluoroacetic acid. Mass spectra were obtained by MALDI-TOF MS using a Voyager-DE Pro mass spectrometer (PerSeptive Biosystems).

### Peptide mapping of $H_2O_2$-treated and inhibitor-bound α-synucleins

Inhibitor-bound α-synuclein monomer and dimer were prepared as described above. For methionine oxidation, α-synuclein monomer (7 mg/mL) was incubated with 0–4% $H_2O_2$ at room temperature for 20 min and then dialyzed

against 30 mM Tris–HCl (pH 7.5) to remove $H_2O_2$. To identify the modification, inhibitor-bound α-synuclein monomer and dimer, as well as $H_2O_2$-treated α-synuclein, were incubated with trypsin at 37 °C for 18 h at an enzyme-to-substrate ratio of 1:50 (mol/mol) in 30 mM Tris–HCl (pH 7.5). Digested peptide products were separated by reverse-phase HPLC on a Supersphere Select B column (2.1 × 125 mm; Merck) and analyzed by MALDI-TOF MS.

### Determination of stoichiometry of exifone/α-synuclein complexes

The stoichiometry of exifone/α-synuclein complexes was determined by measuring the absorbance of exifone at 385 nm using a spectrophotometer (UV-1600 PC, Shimadzu Co). Exifone-bound monomeric and dimeric α-synucleins were isolated by gel-filtration chromatography as described above.

### Redox-cycle staining

Samples were subjected to SDS-PAGE and transferred onto polyvinylidene fluoride membranes. The membranes were incubated in 0.24 mM NBT (Sigma), 2 M potassium glycinate solution (pH 10.0) in the dark for 16 h at room temperature and then dipped in 100 mM sodium borate (pH 10.0). Exifone-bound α-synuclein was specifically stained as purple-blue bands due to NBT reduction to formazan.

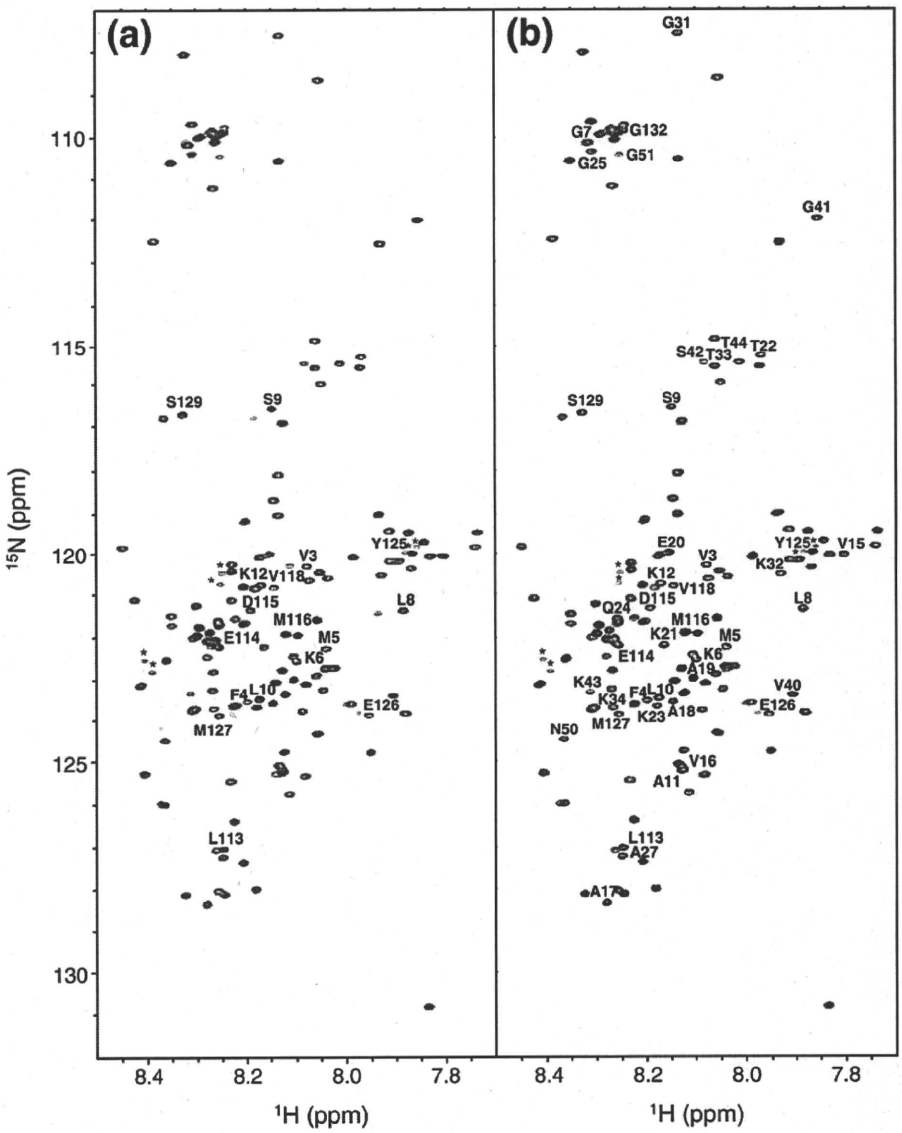


**Fig. 6.** NMR spectral comparison of exifone-bound $^{15}$N-labeled α-synuclein dimer and control monomer. (a) $^{1}$H–$^{15}$N HSQC spectra of $^{15}$N-labeled Exi-monomer (red) and $^{15}$N-labeled control monomer (black) recorded at a proton frequency of 920 MHz. (b) $^{1}$H–$^{15}$N HSQC spectra of $^{15}$N-labeled Exi-dimer (red) and $^{15}$N-labeled control monomer (black). (c) Plot of the relative peak intensities, *I*(Exi-monomer)/*I*(monomer), of the HSQC cross-peaks in the Exi-monomer and control monomer *versus* the amino acid sequence of α-synuclein. (d) *I*(Exi-dimer)/*I*(monomer) of the HSQC cross-peaks in the Exi-dimer and control monomer. Signals derived from oxidized methionines and their neighboring residues (indicated with asterisks in a and b) were split and not taken into account. The peak splittings mostly reflect a mixture of *R* and *S* isomers of methionine sulfoxide.[18]

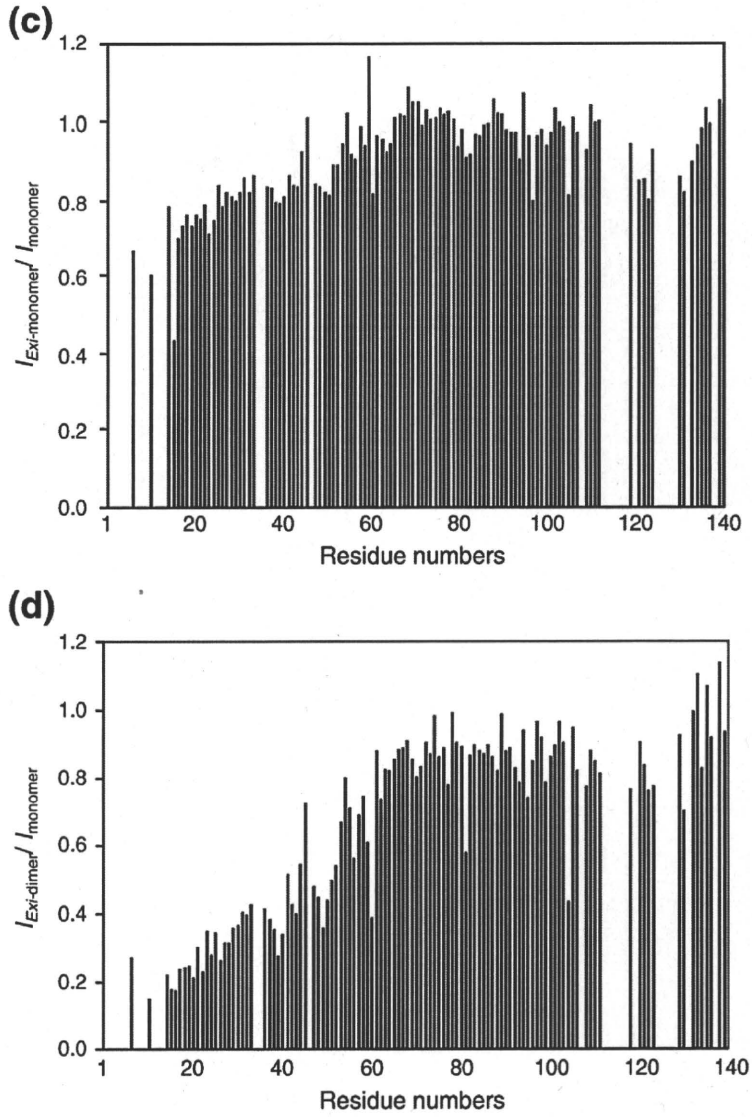


**Fig. 6** *(legend on previous page)*

### Asp-N digestion of α-synuclein dimer

α-Synuclein dimer (0.25 mg/mL) in 30 mM Tris–HCl (pH 7.5) was treated with 40 μg/mL of Asp-N (Roche) at 37 °C for 1 h. The reaction was stopped by adding 2× SDS sample buffer [4% SDS, 0.16 M Tris–HCl (pH 6.8), 30% glycerol] and the solution was boiled for 5 min. The samples were loaded onto 15% Tris/tricine SDS-PAGE gel, and the digested products were detected by silver staining (kit from Wako), immunoblotting, and redox-cycling staining. For immunoblotting, SDS-PAGE gels were blotted onto polyvinylidene fluoride membranes, blocked with 3% gelatin/phosphate-buffered saline, and incubated overnight at room temperature with anti-α-synuclein antibody in 10% FBS/phosphate-buffered saline. After washing, the blots were incubated for 2 h at room temperature with biotinylated secondary antibody (1:500) (Vector Laboratories). Following further washing, the blots were incubated with peroxidase-labeled avidin–biotin (Vector laboratories) for 30 min at room temperature and developed with $NiCl_2$-enhanced diaminobenzidine (Sigma).

### NMR measurements

The samples for NMR experiments were prepared at a concentration of 0.1–1.0 mM in 90% $H_2O$/10% $D_2O$ (v/v), 10 mM sodium phosphate buffer, and 100 mM NaCl at pH 7.0. NMR experiments were performed at 10 °C using a JEOL JNM-ECA920 spectrometer equipped with a 5-mm triple resonance probe. Backbone assignments of α-synuclein monomer were achieved by means of standard triple resonance experiments, as described previously.[13] The samples were checked by SDS-PAGE before and after NMR measurements, and it was confirmed that aggregation of inhibitor-bound α-synuclein monomer and dimer did not occur under these conditions. NMR time domain data were processed with the nmrPipe package[22] and the spectra were analyzed by using

Sparky software (T. D. Goddard and D. G. Kneller, University of California, San Francisco).

## Acknowledgements

We thank K. Senda and K. Hattori (Nagoya City University) for help in the preparation of the recombinant proteins for NMR spectroscopy. We also thank M. Nakano (IMS) and T. Sugihara (JEOL) for help in NMR measurements and K. Matsumoto (RIKEN) for assistance in MS. We thank Drs. H. Sezaki, A. Hayashi, and T. Hosono (Agilent Technologies Japan) for their kind support in liquid chromatography–electrospray ionization MS analysis. This work was supported in part by Grants-in-Aid for Scientific Research on Priority Areas, Research on Pathomechanisms of Brain Disorders (to Y.Y., K.K., and M.H.), Grants-in-Aid for Scientific Research on Innovative Areas, Molecular Science of Fluctuations toward Biological Functions (to K.K.), and "Nanotechnology Network Project" of the Ministry of Education, Culture, Sports, Science and Technology (MEXT). This work was also supported by Takeda Science Foundation (Y.Y.).

## Supplementary Data

Supplementary data associated with this article can be found, in the online version, at doi:10.1016/j.jmb.2009.10.068

## References

1. Conway, K. A., Rochet, J. C., Bieganski, R. M. & Lansbury, P. T., Jr (2001). Kinetic stabilization of the α-synuclein protofibril by a dopamine-α-synuclein adduct. *Science*, **294**, 1346–1349.
2. Li, H. T., Lin, D. H., Luo, X. Y., Zhang, F., Ji, L. N., Du, H. N. *et al.* (2005). Inhibition of α-synuclein fibrillization by dopamine analogs via reaction with the amino groups of α-synuclein. Implication for dopaminergic neurodegeneration. *FEBS J.* **272**, 3661–3672.
3. Masuda, M., Suzuki, N., Taniguchi, S., Oikawa, T., Nonaka, T., Iwatsubo, T. *et al.* (2006). Small molecule inhibitors of α-synuclein filament assembly. *Biochemistry*, **45**, 6085–6094.
4. Porat, Y., Abramowitz, A. & Gazit, E. (2006). Inhibition of amyloid fibril formation by polyphenols: structural similarity and aromatic interactions as a common inhibition mechanism. *Chem. Biol. Drug Des.* **67**, 27–37.
5. Feng, B. Y., Toyama, B. H., Wille, H., Colby, D. W., Collins, S. R., May, B. C. *et al.* (2008). Small-molecule aggregates inhibit amyloid polymerization. *Nat. Chem. Biol.* **4**, 197–199.
6. Norris, E. H., Giasson, B. I., Hodara, R., Xu, S., Trojanowski, J. Q., Ischiropoulos, H. & Lee, V. M. (2005). Reversible inhibition of α-synuclein fibrillization by dopaminochrome-mediated conformational alterations. *J. Biol. Chem.* **280**, 21212–21219.
7. Herrera, F. E., Chesi, A., Paleologou, K. E., Schmid, A., Munoz, A., Vendruscolo, M. *et al.* (2008). Inhibition of α-synuclein fibrillization by dopamine is mediated by interactions with five C-terminal residues and with E83 in the NAC region. *PLoS ONE*, **e3394**, 3.
8. Ehrnhoefer, D. E., Bieschke, J., Boeddrich, A., Herbst, M., Masino, L., Lurz, R. *et al.* (2008). EGCG redirects amyloidogenic polypeptides into unstructured, off-pathway oligomers. *Nat. Struct. Mol. Biol.* **15**, 558–566.
9. Moussa, C. E., Mahmoodian, F., Tomita, Y. & Sidhu, A. (2008). Dopamine differentially induces aggregation of A53T mutant and wild type α-synuclein: insights into the protein chemistry of Parkinson's disease. *Biochem. Biophys. Res. Commun.* **365**, 833–839.
10. Rao, J. N., Dua, V. & Ulmer, T. S. (2008). Characterization of α-synuclein interactions with selected aggregation-inhibiting small molecules. *Biochemistry*, **47**, 4651–4656.
11. Hong, D. P., Fink, A. L. & Uversky, V. N. (2008). Structural characteristics of α-synuclein oligomers stabilized by the flavonoid baicalein. *J. Mol. Biol.* **383**, 214–223.
12. Masuda, M., Hasegawa, M., Nonaka, T., Oikawa, T., Yonetani, M., Yamaguchi, Y. *et al.* (2009). Inhibition of α-synuclein fibril assembly by small molecules: analysis using epitope-specific antibodies. *FEBS Lett.* **583**, 787–791.
13. Sasakawa, H., Sakata, E., Yamaguchi, Y., Masuda, M., Mori, T., Kurimoto, E. *et al.* (2007). Ultra-high field NMR studies of antibody binding and site-specific phosphorylation of α-synuclein. *Biochem. Biophys. Res. Commun.* **363**, 795–799.
14. Uversky, V. N., Yamin, G., Souillac, P. O., Goers, J., Glaser, C. B. & Fink, A. L. (2002). Methionine oxidation inhibits fibrillation of human α-synuclein *in vitro*. *FEBS Lett.* **517**, 239–244.
15. Paz, M. A., Gallop, P. M., Torrelio, B. M. & Fluckiger, R. (1988). The amplified detection of free and bound methoxatin (PQQ) with nitroblue tetrazolium redox reactions: insights into the PQQ-locus. *Biochem. Biophys. Res. Commun.* **154**, 1330–1337.
16. Ingrosso, D., Fowler, A. V., Bleibaum, J. & Clarke, S. (1989). Specificity of endoproteinase Asp-N (Pseudomonas fragi): cleavage at glutamyl residues in two proteins. *Biochem. Biophys. Res. Commun.* **162**, 1528–1534.
17. Tetaz, T., Morrison, J. R., Andreou, J. & Fidge, N. H. (1990). Relaxed specificity of endoproteinase Asp-N: this enzyme cleaves at peptide bonds N-terminal to glutamate as well as aspartate and cysteic acid residues. *Biochem. Int.* **22**, 561–566.
18. Stadtman, E. R., Van Remmen, H., Richardson, A., Wehr, N. B. & Levine, R. L. (2005). Methionine oxidation and aging. *Biochim. Biophys. Acta*, **1703**, 135–140.
19. Rospigliosi, C. C., McClendon, S., Schmid, A. W., Ramlall, T. F., Barre, P., Lashuel, H. A. & Eliezer, D. (2009). E46K Parkinson's-linked mutation enhances C-terminal-to-N-terminal contacts in α-synuclein. *J. Mol. Biol.* **388**, 1022–1032.
20. Jakes, R., Spillantini, M. G. & Goedert, M. (1994). Identification of two distinct synucleins from human brain. *FEBS Lett.* **345**, 27–32.
21. Masuda, M., Dohmae, N., Nonaka, T., Oikawa, T., Hisanaga, S., Goedert, M. & Hasegawa, M. (2006). Cysteine misincorporation in bacterially expressed human α-synuclein. *FEBS Lett.* **580**, 1775–1779.
22. Delaglio, F., Grzesiek, S., Vuister, G. W., Zhu, G., Pfeifer, J. & Bax, A. (1995). NMRPipe: a multidimensional spectral processing system based on UNIX pipes. *J. Biomol. NMR*, **6**, 277–293.

doi:10.1111/j.1479-8301.2010.00318.x PSYCHOGERIATRICS 2010; 10: 69–76

ORIGINAL ARTICLE

# Argyrophilic grain disease with delusions and hallucinations: a pathological study

**Toshiyasu ASAOKA,[1] Kuniaki TSUCHIYA,[2] Hiroshige FUJISHIRO,[3,4] Tetsuaki ARAI,[4] Masato HASEGAWA,[5] Haruhiko AKIYAMA,[4] Eizo ISEKI,[3] Tatsuro ODA,[1] Mitsumoto ONAYA[1] and Itaru TOMINAGA[1]**

[1]Department of Psychiatry, Shimousa Psychiatric Medical Center, Midori-ku, Chiba, [2]Department of Laboratory Medicine and Pathology, Tokyo Metropolitan Matsuzawa Hospital, Setagaya-ku, [3]PET/CT Dementia Research Center, Juntendo Tokyo Koto Geriatric Medical Center, Juntendo University School of Medicine, Koto-ku, [4]Department of Psychogeriatrics, and [5]Department of Molecular Neurobiology, Tokyo Institute of Psychiatry, Setagaya-ku, Tokyo, Japan

*Correspondence:* Dr Hiroshige Fujishiro MD, PhD, PET/CT Dementia Research Center, Juntendo Tokyo Koto Geriatric Medical Center, Juntendo University School of Medicine, 3-3-20 Shinsuna, Koto-ku, Tokyo 136-0075, Japan. Email: fujishiro17@hotmail.co.jp

*Received 6 October 2009; accepted 22 January 2010.*

***Key words:*** *AGD, autopsy, dementia, phosphorylation, psychiatric symptom, tau, TDP-43.*

## Abstract

No clear clinical syndrome for argyrophilic grain disease (AGD) has yet been identified. Previous studies have documented its clinical features, namely, personality changes characterized by emotional disorder involving aggression or ill temper and relatively well-preserved cognitive function, but the clinical manifestations of delusions and hallucinations as they appear in AGD have not been thoroughly described. Here, we report on a 72-year-old Japanese AGD patient who showed psychiatric symptoms, memory impairment and emotional change. He perceived and described a person who was not present and tried to grasp things on the floor though nothing was there. He also insisted that somebody was watching him and consequently always kept his curtains closed. These psychiatric symptoms were observed at an early stage in the patient's disease course. Serial neuroradiological examination showed progressive atrophy of the bilateral temporal lobes. The patient died at 79 years-of-age. Microscopic neuropathological examination showed transactivation responsive region (TAR)-DNA-binding protein of 43 kDa (TDP-43) positive structures in addition to widespread argyrophilic grains and coiled bodies. According to recent recommendations for pathological diagnosis, this case corresponds to AGD with limbic TDP-43 pathology. This case shows that patients with AGD that is eventually confirmed through autopsy can present with delusions and hallucinations early in the course of their disease. The clinical significance of TDP-43 pathology in the brains of patients with AGD remains uncertain.

## INTRODUCTION

Argyrophilic grain disease (AGD) was first described by Braak and Braak in the brains of patients with adult-onset dementia.[1] AGD is neuropathologically characterized by the presence of small spindle- or comma-shaped silver stain-positive structures, so-called argyrophilic grains, in the neuropil in the limbic area, which includes the hippocampus, the entorhinal and transentorhinal cortices and the cingulate cortex.[1-3] Recently, Togo *et al.* classified AGD as 4-repeat tauopathy, such as progressive supranuclear palsy (PSP) and corticobasal degeneration (CBD), based on the morphological, biochemical and genetic analyses.[4,5] Previous studies have documented its clinical features, namely, personality changes characterized by emotional disorder involving aggression or ill temper and relatively well-preserved cognitive function, but the clinical manifestations of delusions and hallucinations as they appear in AGD have not been thoroughly described.[6,7] In the present study, we report the clinical course of an AGD case showing delusions and hallucinations with serial radiological examinations. On neuropathological evaluation, in addition to argyrophilic grains confirmed by modified

Gallyas–Braak staining, detailed immunostaining showed transactivation responsive region (TAR)-DNA-binding protein of 43 kDa (TDP-43) positive structures. The purpose of the present study was to review clinical, radiological and pathological features of this AGD case with TDP-43 immunoreactive pathology, including double-labeling immunofluorescence for phosphorylated tau and phosphorylated TDP-43.

## CASE REPORT

An elderly 79-year-old man had progressive cognitive impairment. He had no family history of dementia or neurological disease. His past medical history included colon cancer, ileus and chronic bronchitis. While he suffered from colon cancer at 72 years-of-age, he presented with delirium after operation. After discharge, he developed memory impairment and fell frequently. He became restless and irritated in the evenings, and requested his wife follow his orders. He perceived and described a person who was not present and tried to grasp things on the floor though nothing was there, suggesting hallucinations. He also insisted that somebody was watching him and consequently always kept his curtains closed. These psychiatric symptoms were observed at an early stage in the patient's disease course. At 74 years of age his symptoms were getting worse, and the patient was admitted to a care unit for dementia in a psychiatric hospital because of his wife's severe burden of taking care of him. At admission, his Mini-Mental State Examination score was 22; orientation of place, 3/5; serial 7, 3/5; remote memory, 0/3; and repetition, 0/1. Computed tomography (CT) of his head showed prominent bilateral inferior ventricle enlargement with slight asymmetry and mild cortical atrophy (Fig. 1a). After hospitalization, he wanted to go home with complaints of inappropriate hospitalization and was uncooperative with medical staff. He was discharged to a health services facility for the elderly several times, but needed to be admitted to a care unit for dementia again because of troubles with other patients, including fighting and stealing. At hospitalization, he lost his temper easily and his social interpersonal conduct declined. When the nurse revealed his stealing to other patients, he apologized and returned the items to them, showing preserved insight into his behavior. He could tell the staff at his bedside his need to urinate a few months before his death. Subsequent head CT showed progressive degeneration of temporal lobes, with relative preservation of the other cortical lobes (Fig. 1b,c). Coronal magnetic resonance imaging (MRI) showed severe temporal atrophy: slightly asymmetric and highly marked atrophy in the anterior mediotemporal lobe 7 months before death (Fig. 2). He died from pneumonia at 79 years-of-age. His clinical duration of dementia was approximately 8 years. Written informed consent from his family was provided before an autopsy was carried out.

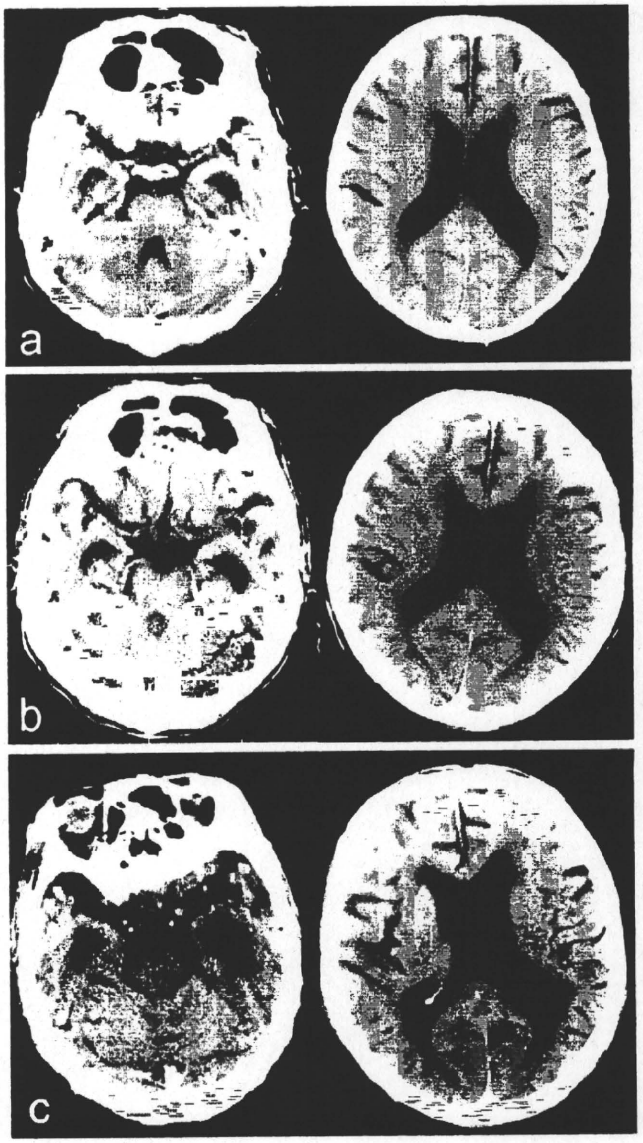


**Figure 1** Computed tomography scans showing progressive enlargement of bilateral inferior ventricles. The temporal lobe showed progressive atrophy, whereas other cortical regions were relatively preserved in the course of the disease. Scans were taken (a) 3 years, (b) 5 years, and (c) 8 years (2 months before death) after the disease onset.

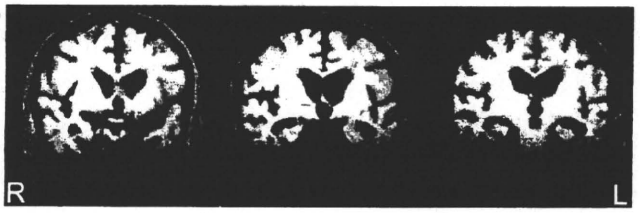


**Figure 2** Magnetic resonance imaging carried out 7 months before death. The temporal lobe, especially the medial portion, had severe atrophy, whereas other cortical regions were relatively preserved.

### Conventional neuropathological examination

Brains tissue samples were fixed postmortem with 10% formaldehyde and embedded in paraffin. Ten-μm-thick sections from the frontal, temporal, parietal, occipital, insular and cingulated cortices, hippocampus, amygdala, basal ganglia, pons, medulla oblongata, and cerebellum were prepared. These sections were stained by hematoxylin–eosin (HE), Klüver–Barrera, methenamine silver and Gallyas–Braak methods. Braak stages of neurofibrillary tangles (NFT) were assigned based on the distribution of NFT seen by modified Gallyas–Braak staining.[8] The degree of amyloid burden was evaluated by using the methenamine silver method.

### Immunohistochemistry

Sections from various regions, including the cerebrum and brainstem, were examined for immunohistochemistry. Deparaffinized and rehydrated sections were immunostained with a monoclonal antibody to phospho-tau (AT8; 1:3000, Innogenetics, Gent, Belgium), a previously well characterized antibody specific for phosphorylated TDP-43 (pS409/410)[9] and a monoclonal antibody to phosphorylated α-synuclein (pSyn#64; 1:3000, Wako, Osaka, Japan) using 3, 3′-diaminobenzidine (DAB) as the chromogen. After immunostaining, the sections were counterstained with hematoxylin.

Double-labeling immunofluorescence for phosphorylated TDP-43 (pS409/410) and phosphorylated tau (AT8; 1:3000, Innogenetics, Gent, Belgium) were carried out using fluorescein isothiocianate (FITC)- and tetramethylrhodamine isothiocyanate (TRITC)-conjugated secondary antibodies; sections were examined with a confocal laser microscope (LSM5 PASCAL; Carl Zeiss MicroImaging GmbH, Jena, Germany).

### Semiquantitative assessment of histopathological lesions

Neuronal loss and gliosis, argyrophilic grains and TDP-43 immunoreactive structures were semiquantitatively evaluated. The degree of degeneration in the cerebral cortex was graded from (–) to (+++): (–), no histopathological alteration; (+), slight neuronal loss and gliosis of the superficial layers; (++), obvious neuronal loss and gliosis found in cortical layers II and III, often accompanied by status spongiosis and relative preservation of neurons in layers V and VI; and (+++), pronounced neuronal loss with gliosis found in all cortical layers, and adjacent subcortical white matter showing prominent fibrillary gliosis. The degree of neuronal loss and gliosis in the basal ganglia and brainstem nuclei was graded from (–) to (+++): (–), no neuronal loss or gliosis observed; (+), mild gliosis observed on HE-stained sections, but no reduction in number of neurons; (++), moderate neuronal loss and gliosis, but no tissue rarefaction; and (+++), severe neuronal loss, severe gliosis and tissue rarefaction observed. The densities of argyrophilic grains in representative regions were graded on Gallyas–Braak-stained sections: (–), no grains; (+), some grains; (++), many grains; and (+++), abundant grains. TDP-43 immunoreactive structures were semi-quantitatively scored from (–) to (+++): (–), absent; (+), mild; (++), moderate; and (+++), severe.

## RESULTS

### Pathological findings

The fixed brain weighed 1280 g. Macroscopic findings showed marked medial temporal atrophy, but mild atrophy of the other neocortical regions. Sequential sections through the supratentorial tissues showed the lateral ventricles to be largely dilated (Fig. 3). The subjacent white matter in the temporal lobe at the level of amygdala showed diffuse gray discoloration. Ambient gyrus was severely affected as previously reported.[10] The substantia nigra and the locus ceruleus had visible pigmentation. The cerebellar sections showed no unusual features.

On microscopic examination, the modified Gallyas–Braak method showed abundant small spindle- or comma-shaped structures, argyrophilic grains (AG) and coiled bodies (CBs) (Fig. 4a) in the neuropil in the limbic area as well as the neocortical regions, mainly the temporal lobe (Fig. 4b,c). The distribution of AG is summarized in Table 1, similar to

that of a previous report.[7] There were some AG in the tegmentum of pons. Neuronal loss with free melanin was observed in the locus celureus. The hippocampus had a normal neuronal population in all sectors of Ammon's horn and just a few scattered NFT in the CA1 region with modified Gallyas–Braak stains. Astrocytosis was present in the endplate and dentate gyrus. The basal nucleus of Meynert had a normal neuronal population and no NFT. The Braak NFT stage was consistent with stage II.[8] There was severe gliosis and neuronal loss with some ballooned neurons in the amygdala on HE (Fig. 4d). Superficial spongiosis was observed in the parahippocampal gyrus, occipitotemporal gyrus and inferior temporal gyrus (Fig. 4e). There were no Pick bodies or Lewy bodies. There was obvious fibrillary gliosis in the cerebral white matter subjacent to the mediotemporal cortex. Widespread diffuse senile plaques were shown by the methenamine silver method, corresponding to pathological aging (Fig. 4f).[11] Brainstem fiber tracts were unremarkable. No neuronal loss was detected in the pontine nucleus, the dorsal vagal nucleus and the inferior olivary nucleus. The cerebellum had no Purkinje cell loss or Bergmann gliosis. No glial cytoplasmic inclusions or Lewy bodies were detected with synuclein immunostaining in the brain.

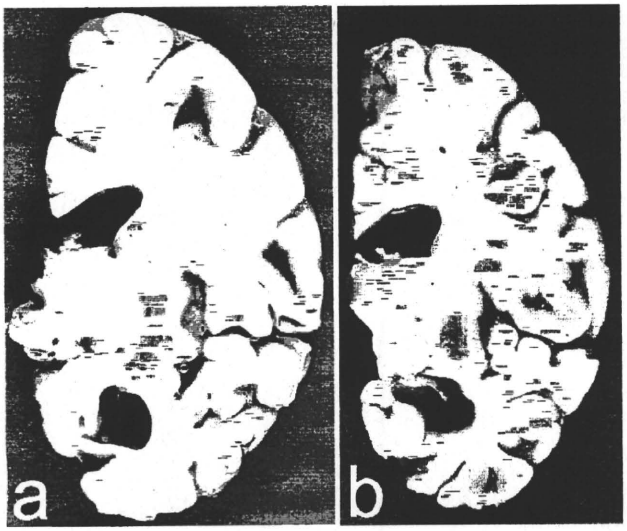


**Figure 3** Macroscopic examination revealed that coronal sections of the left hemisphere showed (a) marked atrophy of the amygdala, entorhinal cortex and adjacent isocortical region of the temporal lobe, and (b) mild atrophy of the hippocampus with relative sparing of the frontal and parietal lobes.

**Immunohistochemistry by using the phosphorylation-dependent anti-TDP-43 antibody**

Before this study, we reported several phosphorylation-specific anti-TDP-43 antibodies.[9] These antibodies react only with abnormally deposited TDP-43 with no nuclear staining, making it easy for us to recognize abnormal findings. Anti-phosphorylated TDP-43 immunohistostaining showed FTLD-TDP-like lesions, including neuronal cytoplas-

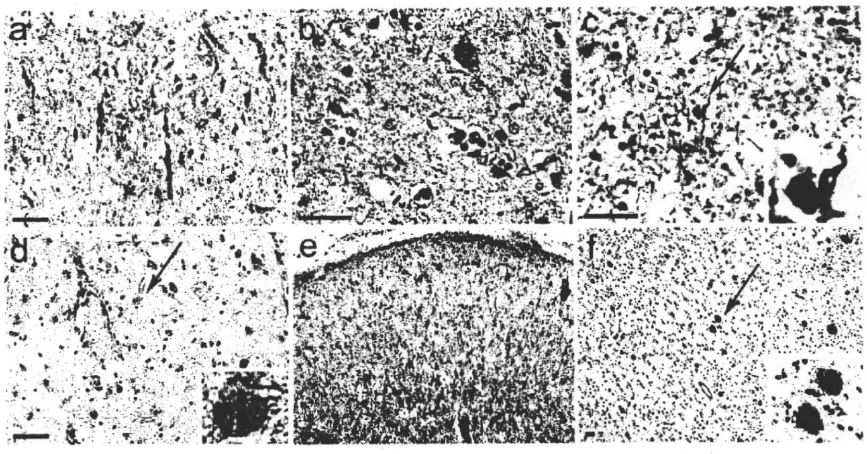


**Figure 4** Microscopic findings using conventional methods. The modified Gallyas–Braak method shows argyrophilic grains and coiled bodies not only in (a) the limbic regions, but also in (b) the temporal cortex and (c) subjacent white matter. (d) Ballooned neurons and neuronal loss with gliosis in the amygdala and (e) spongy changes in the cortex were observed on HE staining. (f) The methenamine silver method showed numerous diffuse plaques in the temporal cortex (f). (a) Entorhinal cortex, (b) superior temporal gyrus, (c) temporal white matter, (d) amygdala, (e) occipitotemporal cortex and (f) inferior temporal cortex. The inset in the lower right corner of (c) (d) and (f) represents a higher magnification of the region indicated by an arrow. Bars, 50 μm.

**Table 1** Distribution of argyrophilic grains and TDP43-immunoreactive structures

| Region | Neuronal loss/gliosis | Argyrophilic grain | TDP43-positive structure |
|---|---|---|---|
| Frontal cortex | | | |
| Superior frontal gyrus (ant/post) | –/– | –/– | –/– |
| Middle frontal gyrus (ant/post) | – | –/– | –/– |
| Inferior frontal gyrus (ant/post) | – | –/– | –/– |
| Orbital gyrus | – | + | Not examined |
| Rectal gyrus | – | + | Not examined |
| Temporal cortex | | | |
| Superior temporal gyrus (ant/post) | –/– | +/+ | –/– |
| Middle temporal gyrus (ant/post) | +/– | ++/+ | +/– |
| Inferior temporal gyrus (ant/post) | ++/+ | +++/++ | ++/+ |
| Parietal cortex | – | + | – |
| Occipital cortex | – | – | Not examined |
| Insular cortex (ant/post) | ++/– | ++/– | –/– |
| Cingulate (ant/post) | +/– | ++/– | –/– |
| Amygdala | | | |
| Corticomedialis | ++ | +++ | +++ |
| Basolateral | +++ | +++ | +++ |
| Hippocampus | | | |
| CA1 | – | +++ | + |
| CA2 | – | ++ | + |
| CA4 | –† | + | + |
| Dentate gyrus | –† | + | + |
| Subiculum | – | +++ | + |
| Parahippocampal gyrus (ant/post) | ++/+ | +++/++ | ++/+ |
| Caudate/putamen | –/– | –/– | –/– |
| Globus pallidus | – | – | – |
| Thalamus | – | + | – |
| Hypothalamus | Difficult to evaluate | +++ | + |
| Subthalamic nucleus | – | + | – |
| Basal forebrain | Difficult to evaluate | + | – |
| Substantia nigra | Not examined | Not examined | Not examined |
| Locus celureus | + | + | Not examined |
| Pontine nucleus | – | – | Not examined |
| Dosal vagal nucleus | – | – | Not examined |
| Inferior olivary nucleus | – | – | Not examined |
| Cerebellum | – | – | Not examined |

Ant, at the level of the anterior commisure; post, at the level of the lateral geniculate body. †Astrocytosis without neuronal loss was present.

mic inclusions, dystrophic neurites and glial cytoplasmic inclusions (Fig. 5b,c). There was no neuronal intranuclear inclusion. TDP-43-positive neuronal cytoplasmic inclusion in the dentate gyrus of the hippocampus, which is one of the features of FTLD-TDP, was observed (Fig. 5c). In addition to these FTLD-TDP-like lesions, some grain-like structures were found to be positive for TDP-43 (Fig. 5a). The distribution and severity of TDP-43 immunoreactive structures were largely parallel with those of AG, as detailed in Table 1. There were neither AG nor TDP-43-positive structures in the striatum. According to recent consensus recommendation for pathological diagnosis, the present case corresponds to AGD with limbic TDP-43 pathology.[12]

### Colocalization of TDP-43 immunoreactive structures and tau-positive structures

In the entorhinal cortex and the amygdala, occasional colocalization of phospho-tau and phospho-TDP-43 was observed in the neuronal cytoplasmic inclusions and grain-like structures in the neuropil (Fig. 6a-c). However, the majority of phosphorylated TDP-43 aggregates were not colocalized with phospho-tau staining.

## DISCUSSION

We described a case of AGD with delusions and hallucinations at an early stage in the disease course. Because this patient's psychiatric symptoms

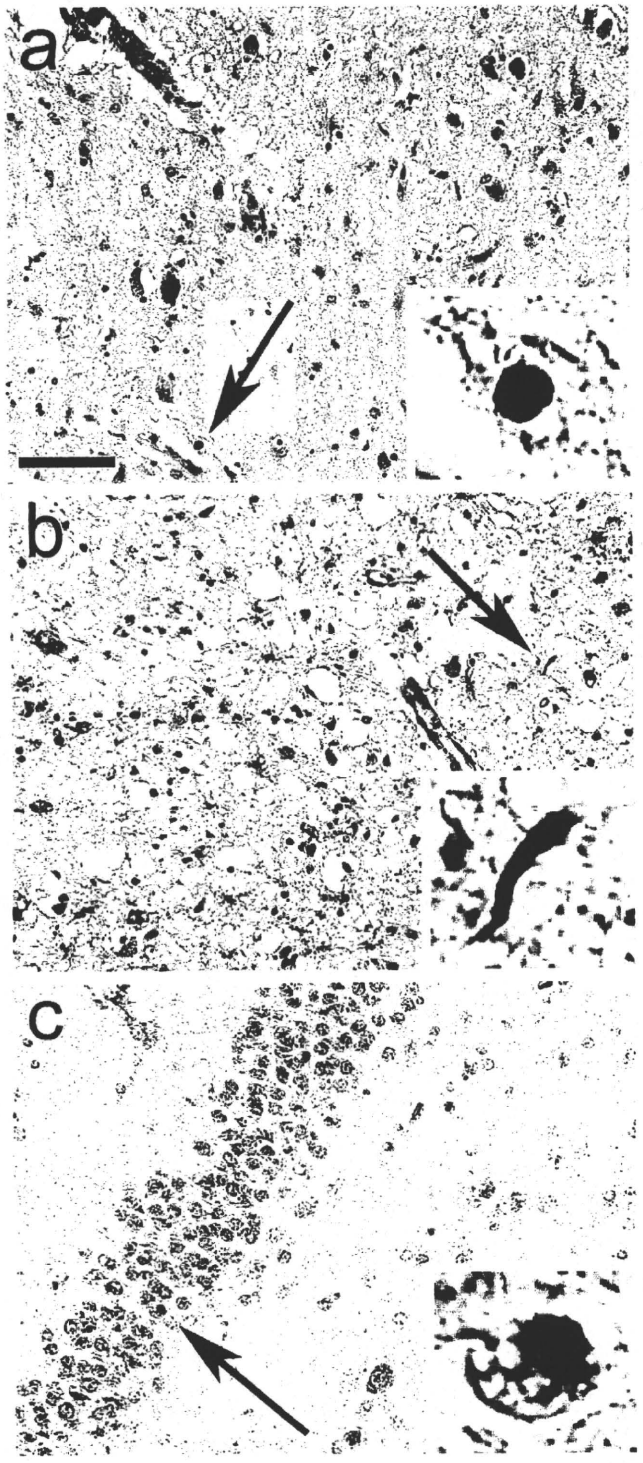


**Figure 5** Immunohistochemistry of argyrophilic grain disease using the phosphorylation-dependent anti-TDP-43 antibody (pS409/410). Phosphorylation-dependent TDP-43 immunohistochemistry shows (a) grain-like structures as well as (b) dystrophic neurites and (c) neuronal cytoplasmic inclusions. (a) Amygdala, (b) occipitotemporal cortex, and (c) dentate gyrus of hippocampus. The inset in the lower right corner of each image represents a higher magnification of the region indicated by an arrow. Bars, 50 μm.

persisted, it is unlikely that they were the result of delirium.

To date, few reports have described the delusions and hallucinations seen in cases of AGD. Ikeda *et al.* described the clinical courses of four patients with autopsy-confirmed AGD and identified personality changes characterized by emotional disorder with aggression or ill temper and relatively well-preserved cognitive function as the clinical features.[7] Two of these four cases showed delusions and hallucinations at early stages of the disease course; one had delusions of robbery and the other showed both delusions and hallucinations, saying things like, 'they speak ill of me' and 'someone is in the house'. Togo *et al.* documented the clinical features of AGD cases who were admitted to geriatric wards of psychogeriatric hospitals. In 10 AGD cases with concurrent mild Alzheimer pathology, the most common initial symptom was amnesia (70%), whereas delusions were usually observed within 3 years after disease onset (70%).[6] Only one patient showed hallucinations as the initial symptom. Both studies have suggested that, in addition to amnesia, delusions and hallucinations can occur at early stages of the disease course. It is of interest that the emergence of these psychiatric symptoms precedes the appearance of amnesia in some AGD cases,[6,7] especially because Saito *et al.* reported that argyrophilic grains are initially found in the temporo-amygdaloid junction, and that the distribution of argyrophilic grains followed a stereotypic regional pattern reflecting an antero-posterior gradient in the putative progression of AGD.[13] The clinical features reported in these studies are largely consistent with those seen in the present case, although in our case hallucinations were relatively rare. It should be noted that these other studies might have overestimated the frequency of delusions and hallucinations in AGD, because the AGD patients in these studies were admitted to psychiatric hospitals.

In a neuropathological examination of the present patient, modified Gallyas–Braak staining confirmed abundant argyrophilic grains and coiled bodies; these findings are consistent with his diagnosis of AGD. Furthermore, detailed immunostaining showed TDP-43-positive structures. According to a recent

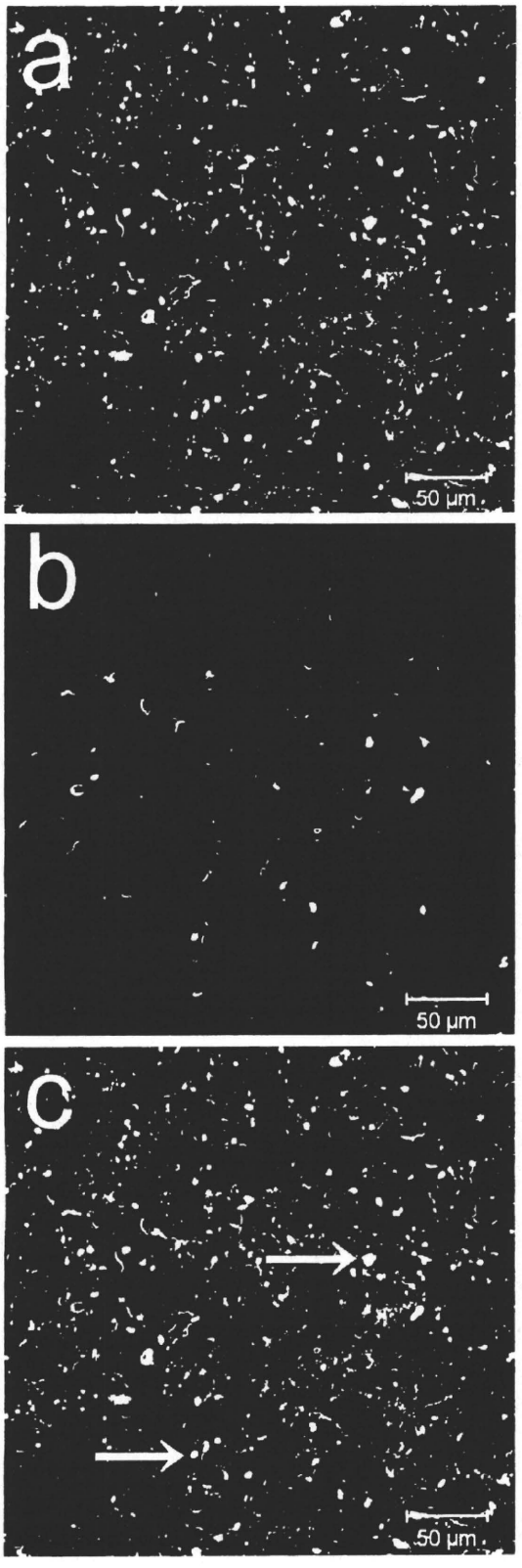


**Figure 6** Confocal double-immunofluorescence of phospho-tau and phospho-TDP-43. In the entorhinal cortex, (a) many grains and neurons are positive for tau, and (b) small dot-like structures, short dystrophic neurites and round inclusions are immunopositive for TDP-43. Merged images are shown in (c). Occasional colocalization is seen in some grain-like structures in the neuropil and neuronal cytoplasmic inclusions (yellow) in (c) (arrows).

consensus recommendation for pathological diagnosis, the present case corresponds to AGD with limbic TDP-43 pathology. Other recent studies have reported that TDP-43 immunoreactivity co-occurs to various degrees with a variety of neurodegenerative disorders, including Alzheimer's disease, Lewy body disease, hippocampal sclerosis, corticobasal degeneration, Guamanian ALS/PDC, Huntington's disease and argyrophilic grain disease.[14–23] The clinical significance of TDP-43 pathology in the brains of patients with various neurodegenerative disorders remains uncertain. Some studies have reported a higher than average age at death in TDP-43-positive cases with both Alzheimer's disease and Lewy related disorders.[15,16] In contrast, Uryu *et al.* reported that there was no clinical difference between Alzheimer's disease with and without TDP-43 immunoreactivity.[17] Our previous study likewise showed no difference in disease duration or age at death between AGD cases with and those without TDP-43 immunoreactivity.[23] Additional clinical features should be examined in detail to clarify the clinical significance of TDP-43 pathology.

## ACKNOWLEDGEMENTS

This work was supported by a Grant-in-Aid for Young Scientists (B) 21791142 by the Ministry of Education, Culture, Sports, Science and Technology in Japan. The assistance of Chie Haga and Hiromi Kondo for histological and immunohistochemistry studies is greatly appreciated.

## REFERENCES

1 Braak H, Braak E. Argyrophilic grains: Characteristic pathology of cerebral cortex in cases of adult onset dementia without Alzheimer changes. *Neurosci Lett* 1987; **76**: 124–127.
2 Braak H, Braak E. Cortical and subcortical argyrophilic grains characterize a disease associated with adult onset dementia. *Neuropathol Appl Neurobiol* 1989; **15**: 13–26.
3 Ferrer I, Santpere G, van Leeuwen FW. Argyrophilic grain disease. *Brain* 2008; **131**: 1416–1432.
4 Togo T, Sahara N, Yen SH *et al.* Argyrophilic grain disease is a sporadic 4-repeat tauopathy. *J Neuropathol Exp Neurol* 2002; **61**: 547–556.

5 Togo T, Cookson N, Dickson DW. Argyrophilic grain disease: Neuropathology, frequency in a dementia brain bank and lack of relationship with apolipoprotein E. *Brain Pathol* 2002; **12**: 45–52.
6 Togo T, Isojima D, Akatsu H *et al.* Clinical features of argyrophilic grain disease: A retrospective survey of cases with neuropsychiatric symptoms. *Am J Geriatr Psychiatry* 2005; **13**: 1083–1091.
7 Ikeda K, Akiyama H, Arai T, Matsushita M, Tsuchiya K, Miyazaki H. Clinical aspects of argyrophilic grain disease. *Clin Neuropathol* 2000; **19**: 278–284.
8 Braak H, Braak E. Neuropathological staging of Alzheimer-related changes. *Acta Neuropathol* 1991; **82**: 239–259.
9 Hasegawa M, Arai T, Nonaka T *et al.* Phosphorylated TDP-43 in frontotemporal lobar degeneration and amyotrophic lateral sclerosis. *Ann Neuro* 2008; **64**: 60–70.
10 Saito Y, Yamazaki M, Kanazawa I, Murayama S. Severe involvement of the ambient gyrus in a case of dementia with argyrophilic grain disease. *J Neurol Sci* 2002; **196**: 71–75.
11 Dickson DW, Crystal HA, Mattiace LA *et al.* Identification of normal and pathological aging in prospectively studied nondemented elderly humans. *Neurobiol Aging* 1992; **13**: 179–189.
12 Mackenzie IR, Neumann M, Bigio EH *et al.* Nomenclature for neuropathologic subtypes of frontotemporal lobar degeneration: Consensus recommendations. *Acta Neuropathol* 2009; **117**: 15–18.
13 Saito Y, Ruberu NN, Sawabe M *et al.* Staging of argyrophilic grains: An age-associated tauopathy. *J Neuropathol Exp Neurol* 2004; **63**: 911–918.
14 Amador-Ortiz C, Lin WL, Ahmed Z *et al.* TDP-43 immunoreactivity in hippocampal sclerosis and Alzheimer's disease. *Ann Neurol* 2007; **61**: 435–445.
15 Arai T, Mackenzie IR, Hasegawa M *et al.* Phosphorylated TDP-43 in Alzheimer's disease and dementia with Lewy bodies. *Acta Neuropathol* 2009; **117**: 125–136.
16 Nakashima-Yasuda H, Uryu K Robinson J *et al.* Co-morbidity of TDP-43 proteinopathy in Lewy body related diseases. *Acta Neuropathol* 2007; **114**: 221–229.
17 Uryu K, Nakashima-Yasuda H, Forman MS *et al.* Concomitant TAR-DNA-binding protein 43 pathology is present in Alzheimer disease and corticobasal degeneration but not in other tauopathies. *J Neuropathol Exp Neurol* 2008; **67**: 555–564.
18 Geser F, Winton MJ, Kwong LK *et al.* Pathological TDP-43 in parkinsonism-dementia complex and amyotrophic lateral sclerosis of Guam. *Acta Neuropathol* 2008; **115**: 133–145.
19 Hasegawa M, Arai T, Akiyama H *et al.* TDP-43 is deposited in the Guam parkinsonism-dementia complex brains. *Brain* 2007; **130**: 1386–1394.
20 Higashi S, Iseki E, Yamamoto R *et al.* Concurrence of TDP-43, tau and alpha-synuclein pathology in brains of Alzheimer's disease and dementia with Lewy bodies. *Brain Res* 2007; **1184**: 284–294.
21 Freeman SH, Spires-Jones T, Hyman BT, Growdon JH, Frosch MP. TAR-DNA binding protein 43 in Pick disease. *J Neuropathol Exp Neurol* 2008; **67**: 62–67.
22 Schwab C, Arai T, Hasegawa M, Yu S, McGeer PL. Colocalization of TDP-43 and huntingtin in inclusions of Huntington's disease. *J Neuropathol Exp Neurol* 2008; **67**: 1159–1165.
23 Fujishiro H, Uchikado H, Arai T *et al.* Accumulation of phosphorylated TDP-43 in brains of patients with argyrophilic grain disease. *Acta Neuropathol* 2009; **117**: 151–158.

Acta Neuropathol (2010) 119:689–702
DOI 10.1007/s00401-010-0664-3

ORIGINAL PAPER

# Multi-organ distribution of phosphorylated α-synuclein histopathology in subjects with Lewy body disorders

**Thomas G. Beach · Charles H. Adler · Lucia I. Sue · Linda Vedders · LihFen Lue · Charles L. White III · Haru Akiyama · John N. Caviness · Holly A. Shill · Marwan N. Sabbagh · Douglas G. Walker · Arizona Parkinson's Disease Consortium**

Received: 17 December 2009 / Revised: 11 February 2010 / Accepted: 26 February 2010 / Published online: 21 March 2010


**Abstract** A sensitive immunohistochemical method for phosphorylated α-synuclein was used to stain sets of sections of spinal cord and tissue from 41 different sites in the bodies of 92 subjects, including 23 normal elderly, 7 with incidental Lewy body disease (ILBD), 17 with Parkinson's disease (PD), 9 with dementia with Lewy bodies (DLB), 19 with Alzheimer's disease with Lewy bodies (ADLB) and 17 with Alzheimer's disease with no Lewy bodies (AD-NLB). The relative densities and frequencies of occurrence of phosphorylated α-synuclein histopathology (PASH) were tabulated and correlated with diagnostic category. The greatest densities and frequencies of PASH occurred in the spinal cord, followed by the paraspinal sympathetic ganglia, the vagus nerve, the gastrointestinal tract and endocrine organs. The frequency of PASH within other organs and tissue types was much lower. Spinal cord and peripheral PASH was most common in subjects with PD and DLB, where it appears likely that it is universally widespread. Subjects with ILBD had lesser densities of PASH within all regions, but had frequent involvement of the spinal cord and paraspinal sympathetic ganglia, with less-frequent involvement of end-organs. Subjects with ADLB had infrequent involvement of the spinal cord and paraspinal sympathetic ganglia with rare involvement of end-organs. Within the gastrointestinal tract, there was a rostrocaudal gradient of decreasing PASH frequency and density, with the lower esophagus and submandibular gland having the greatest involvement and the colon and rectum the lowest.

**Keywords** Parkinson's disease · Parkinsonism · Dementia with Lewy bodies · Alzheimer's disease · Incidental Lewy bodies · α-Synuclein · Spinal cord · Sympathetic nervous system · Peripheral nervous system · Autonomic nervous system · Enteric nervous system · Submandibular gland · Esophagus · Adrenal gland · Heart · Stomach · Gastrointestinal system

## Introduction

The topographical distribution and density of Lewy bodies and their associated abnormal neurites are much greater than formerly appreciated [8, 28, 31, 33, 37, 44, 46, 61, 64, 70, 71, 77, 82]. Furthermore, it is also now more clearly apparent that Lewy body pathology frequently extends to the spinal cord and peripheral nervous system [12, 14, 17–19, 29, 40, 48, 81]. Despite these recent achievements, there has not yet been published a wide survey of the distribution of Lewy-type histopathological changes in the peripheral nervous system. A sensitive immunohistochemical method for phosphorylated α-synuclein [8, 10]

**Electronic supplementary material** The online version of this article (doi:10.1007/s00401-010-0664-3) contains supplementary material, which is available to authorized users.

T. G. Beach (✉) · L. I. Sue · L. Vedders · L. Lue · H. A. Shill · M. N. Sabbagh · D. G. Walker
Sun Health Research Institute, 10515 West Santa Fe Drive, Sun City, AZ 85351, USA
e-mail: thomas.beach@bannerhealth.com

C. H. Adler · J. N. Caviness
Mayo Clinic, Scottsdale, AZ, USA

C. L. White III
University of Texas Southwestern Medical Center, Dallas, TX, USA

H. Akiyama
Tokyo Institute of Psychiatry, Tokyo, Japan

was used to stain sets of spinal cord and peripheral nervous system sections from 92 subjects that had previously received neuropathological diagnoses and Lewy body central nervous system (CNS) staging. The densities and frequencies of occurrence of phosphorylated α-synuclein histopathology (PASH) in multiple regions of spinal cord, sympathetic ganglia and tissue from the major organ systems were tabulated and correlated with diagnostic category. The results are presented below.

## Materials and methods

### Human subjects

Deceased human subjects were autopsied at Sun Health Research Institute (SHRI), a division of the not-for-profit health care provider Banner Health, located in the Sun Cities retirement communities of northwest metropolitan Phoenix, Arizona. All subjects had volunteered for the SHRI Brain and Body Donation Program (BBDP) [5, 9]. The majority of BBDP subjects are clinically characterized at SHRI with annual standardized test batteries that include functional, neuropsychological and neuromotor components, including the Mini Mental State Examination (MMSE) and Unified Parkinson's Disease Rating Scale (UPDRS). In addition, private medical records are requisitioned and reviewed for each subject and the postmortem Dementia Questionnaire [32] or an adaptation of the Clinical Dementia Rating Scale (CDR) are administered to subject contacts to help determine the presence or absence of dementia for those subjects lacking standardized antemortem evaluations. Subjects sign consent that has been approved by the Banner Health Institutional Review Board.

Subjects were chosen by searching the BBDP database for all cases that had received a whole-body autopsy, a completed neuropathologist's examination and a neuropathologic diagnosis of a Lewy body disorder, including Parkinson's disease (PD), dementia with Lewy bodies (DLB), incidental Lewy body disease (ILBD) and Alzheimer's disease with Lewy bodies (ADLB). Comparison groups were composed of subjects without evidence of dementia or parkinsonism (normal elderly subjects) and subjects with AD but no Lewy body pathology (ADNLB).

Subjects received standardized neuropathological examinations. Specific clinicopathologic diagnostic criteria were used for AD [1], PD [36], and DLB [58]. For both AD and DLB, cases received the diagnosis if they were classified as "intermediate" or "high" probabilities in their respective classification schemes. Cases with PASH, but not meeting these diagnostic criteria were designated as either ILBD, if they had no clinical history of parkinsonism or dementia, or ADLB if they had dementia, Alzheimer's disease and Lewy bodies in any brain region, but failed to meet clinicopathologic criteria for DLB or PD.

Gross and microscopic neuropathologic assessments were made by a single observer (TGB) without knowledge of the clinical history or clinical diagnosis; subsequently the clinical history was reviewed with the neurologists (CHA, JNC, HAS, MNS) in order to make an appropriate clinicopathologic diagnosis.

### Histologic methods

Diagnostic histologic methods were performed on standard blocks of tissue that were fixed in 3.75% neutral-buffered formaldehyde and then either dehydrated and embedded in paraffin or cryoprotected and cut on a freezing, sliding microtome. Each case was first staged according to the Unified Staging System for Lewy body disorders with a standard set of brain sections stained with an immunohistochemical method for phosphorylated α-synuclein as previously described [8]. The Unified Staging System is a modification of the scheme first devised by the Dementia with Lewy Bodies Consortium [8, 58, 59].

Paraffin-embedded sections from multiple body sites (Table 1) were stained in an identical fashion as the brain sections, using a polyclonal antiserum raised against an α-synuclein peptide fragment phosphorylated at serine 129, after epitope exposure with proteinase K [34]. The process leading to the choice of immunohistochemical method, as well as details of the method, has been described in a previous publication [10]. In each body region, the density of α-synuclein-immunoreactive perikaryal neuronal cytoplasmic inclusions as well as puncta and neurites was scored, at the site of highest density, by a single observer (TGB) without knowledge of diagnosis, as none, sparse, moderate, frequent and very frequent, using the templates provided by the Dementia with Lewy Bodies Consortium [58]. The total number of body sites examined varied between subjects as an initially broad sampling scheme was progressively reduced to those regions showing a greater likelihood to have positive staining. To evaluate the relative frequency of immunoreactivity in the different body regions, paraffin sections on a single stained slide from each body site listed in Table 1 were used. Following this analysis, selected regions of interest were further evaluated with up to five additional paraffin sections and/or 80 μm thick formalin-fixed, frozen sections.

Alzheimer's disease histopathology was staged and graded on 40 μm thick sections stained with the Gallyas method for neurofibrillary tangles and the Campbell–Switzer and thioflavine-S methods for senile plaques [15]. Braak's neurofibrillary tangle stages and CERAD neuritic plaque densities were assigned as described [16, 62].

**Table 1** Body sites, organs and tissue types investigated with an immunohistochemical method for phosphorylated α-synuclein histopathology

| Body region | Sites investigated within region |
|---|---|
| Spinal cord | Cervical (C4–5), thoracic (T6–7), lumbar (L3–4) and sacral (S1–5) spinal cord |
| Sympathetic ganglia | Middle cervical ganglia, middle ganglia of thoracic chain |
| Vagus nerve | Alongside the common carotid artery at the level of the larynx |
| Sciatic nerve | Overlying the external iliac artery in the pelvic cavity |
| Gastrointestinal system | Upper third and lower third of esophagus, stomach (body), duodenum, jejunum, ileum, transverse colon, sigmoid colon, rectum, submandibular gland, liver, pancreas (head), gallbladder |
| Respiratory system | Larynx, primary bronchus, lung |
| Endocrine system | Adrenal gland, thyroid gland, parathyroid gland, ovary, testis |
| Cardiovascular system | Thoracic and abdominal aorta, left and right ventricle and epicardium of heart at apex |
| Genitourinary tract | Kidney, urinary bladder, uterus, vagina |
| Musculoskeletal system | Rib (bone and associated muscle and soft tissue), psoas muscle, diaphragm |
| Skin | Abdominal skin, scalp |
| Miscellaneous | Spleen, lymph nodes (parabronchial), small bowel mesentery, breast |

### Statistical analysis

Statistical analyses consisted of, for comparing group means, analysis of variance (ANOVA), or, for non-parametric data, Kruskall–Wallis ANOVA. Proportional measures were compared using $\chi^2$ tests.

## Results

Ninety-two subjects had a full autopsy as well as neuropathological diagnoses within the targeted groups. All data from the study are given within the supplementary online table, for brevity some of the data are grouped for summary here. Descriptive measures of these groups are given in Tables 2, 3 and 4. The subjects were all of advanced age (Table 2) and the group means differed significantly ($P < 0.0001$), with the youngest group (PD) having a mean age of 79.3 while the oldest group (ILBD) mean was 86.7. As with all subjects of this advanced age, all had at least some neurofibrillary tangles in the brain [13] and even the elderly control group had a mean Braak stage of 2.6. All diagnostic groups had more male subjects and this was pronounced in the PD and DLB groups. The median postmortem intervals were uniformly short, ranging from 2.7 to 5.9 h and the group means were not significantly different.

The distribution of PASH within the brain is summarized in Table 3 using the Unified Staging System for Lewy Body Disorders and the mean densities of PASH within the ten scored brain regions are given in Table 4. An estimate of the aggregate CNS load of microscopic disease was also determined, using the sum of the mean PASH density scores in all ten evaluated brain regions (Table 4).

**Table 2** General characteristics of the study subjects, by neuropathologic diagnosis, age, gender, postmortem interval (PMI), Braak neurofibrillary stage and CERAD neuritic plaque (NP) density

| Diagnosis (*N*) | Age[a] | Gender (% male) | PMI (h) | Braak stage[a] | CERAD NP density[a] |
|---|---|---|---|---|---|
| Normal (23) | 81.0 (14.1) | 56.5 | 3.9 (2.5) | 2.6 (1.3) | 1.0 (1.3) |
| ILBD (7) | 86.7 (8.5) | 57.1 | 3.8 (2.9) | 3.0 (1.0) | 1.3 (1.4) |
| PD (17) | 79.3 (7.5) | 76.5 | 4.9 (4.1) | 2.5 (1.1) | 0.8 (1.2) |
| DLB (9) | 83.2 (9.5) | 67 | 2.7 (0.4) | 4.4 (0.7) | 3.0 (0.0) |
| ADLB (19) | 84.0 (5.0) | 53.0 | 4.3 (3.8) | 5.2 (1.0) | 2.7 (0.7) |
| ADNLB (17) | 84 (5.9) | 53.0 | 5.9 (10.2) | 4.4 (1.2) | 2.8 (0.4) |

Means and standard deviations (SD) are given

Subjects did not differ significantly in terms of gender distribution or PMI but differed significantly in terms of age, Braak stage and CERAD neuritic plaque density

[a] Group means were significantly different ($P < 0.0001$)

**Table 3** Classification of subjects with phosphorylated α-synuclein histopathology by the Unified Staging System for Lewy body disorders

| Diagnosis | Olfactory bulb only (I) | Brainstem predominant (IIa) | Limbic predominant (IIb) | Brainstem and limbic (III) | Neocortical (IV) |
|---|---|---|---|---|---|
| ILBD[a] | 0 | 1 (17%) | 2 (33%) | 3 (50%) | 0 |
| PD[a] | 0 | 2 (12.5%) | 0 | 10 (62.5%) | 4 (25%) |
| DLB | 0 | 0 | 0 | 1 (11%) | 8 (89%) |
| ADLB | 2 (10%) | 3 (16%) | 11 (58%) | 3 (16%) | 0 |

Number and percentage of subjects in each stage are given

[a] One subject was not classifiable due to missing brain regions needed for staging

**Table 4** Mean (SD) of phosphorylated α-synuclein histopathology regional brain density scores for all subjects by diagnostic classification, with an aggregate total brain load (last row) given by the sum of the mean regional density scores

| Brain region | ILBD | PD | DLB | ADLB |
|---|---|---|---|---|
| Olfactory bulb | 2.5 (1.0) | 2.6 (0.9) | 3.6 (1.1) | 3.0 (0.9) |
| Medulla | 1.6 (1.6) | 3.2 (0.7) | 3.4 (0.7) | 1.0 (1.2) |
| Pons | 1.1 (1.5) | 3.0 (0.9) | 3.1 (1.0) | 0.3 (0.6) |
| Midbrain | 0.4 (0.8) | 3.0 (0.9) | 2.9 (1.5) | 0.2 (0.7) |
| Amygdala | 2.5 (1.6) | 3.1 (0.9) | 3.9 (0.3) | 2.4 (1.7) |
| Transentorhinal | 0.8 (1.8) | 2.3 (1.1) | 3.6 (0.7) | 2.4 (1.8) |
| Cingulate cortex | 0.3 (0.8) | 1.8 (1.0) | 2.9 (1.2) | 0.3 (0.4) |
| Mid. temp. gyrus | 0.3 (0.5) | 1.2 (1.1) | 2.6 (0.9) | 0.2 (0.4) |
| Mid. front. gyrus | 0.3 (0.5) | 1.1 (0.9) | 1.7 (1.1) | 0.05 (0.2) |
| Inf. par. lobule | 0.3 (0.5) | 1.0 (1.0) | 1.8 (1.0) | 0.05 (0.2) |
| Sum of mean scores | 10.1 | 22.3 | 29.5 | 9.9 |

More than 80% of subjects with PD and DLB were in the two highest stages, involving either brainstem through limbic regions (Stage III) or brainstem through neocortical regions (Stage IV). Most subjects with ILBD were in the brainstem-predominant (IIa) or limbic-predominant (IIb) stages while the most frequent stage for ADLB subjects was limbic predominant (IIb). Subjects with ILBD and ADLB had similar overall low aggregate PASH load scores while subjects with PD and DLB had overall high aggregate PASH load scores.

Figure 1 shows photomicrographs of the immunohistochemical staining for α-synuclein in the spinal cord, sympathetic ganglia and vagus nerve. Generally, sections with positive staining contained fibers, puncta and neuronal perikaryal staining (a, c, e, f, h) but occasionally sections or regions contained just fibers (i) or just perikaryal staining. The perikaryal staining was either diffusely distributed in the cytoplasm (e) or condensed into defined inclusions (h), only a subset of which resembled classical Lewy bodies. Within the vagus and peripheral nerves, and generally within nerves seen elsewhere in other body regions, positive staining was only in the form of nerve fibers (i). Within the spinal cord, positively-stained structures were found in all gray matter regions, including posterior horn (b, c), anterior horn (d, e), intermediolateral region (a) and adjacent to the central canal (f). Although not formally analyzed here, the most frequent regions affected appeared to be the thoracolumbar intermediolateral horn and the base of the posterior horn of the sacral cord.

Figure 2 shows photomicrographs of the immunohistochemical staining for α-synuclein in multiple bodily organs and tissue types. As described for the spinal cord and sympathetic ganglia above, sections with positive staining contained either fibers, puncta or neuronal (ganglion cell) perikaryal staining, but ganglion cell staining was much less frequently seen, with the great majority of immunoreactive elements being fibers and puncta. A much more detailed morphologic delineation was seen in 80-μm thick sections of submandibular gland and lower esophagus (Fig. 3), where extensive fiber networks and moderately frequent ganglion cells were often visualized, especially in subjects with PD or DLB. Generally, immunoreactive structures in the gastrointestinal tract were concentrated in the myenteric plexus of Auerbach and the submucosal plexus of Meissner. In the submandibular gland and pancreas, positively stained elements tended to be concentrated in nerve bundles within the connective tissue stroma. In the submandibular gland, 80-μm section staining occasionally showed nerve fibers apparently investing arterioles (Fig. 3d). Adrenal gland staining was exclusively seen in the medulla and in nerve bundles in the surrounding fatty tissue, with no staining seen in the adrenal cortex.

The regional distribution of PASH, as evaluated in single microscopic slides from each body site, is shown in Table 5 and Fig. 4. No immunoreactive elements were present in any subject that had previously been classified, on the basis of the brain examination, as being free of PASH. Subjects with DLB and PD had similar profiles (Fig. 4b, c) and will be discussed together. In both the groups, the most frequently affected body region was the spinal cord, with 25 of 26 subjects involved, followed by the sympathetic ganglia (19/24), the vagus nerve (15/21), the gastrointestinal system (16/26), the sciatic nerve (10/22) and endocrine system (5/14), with other organ systems and tissues following at generally much lower frequencies.

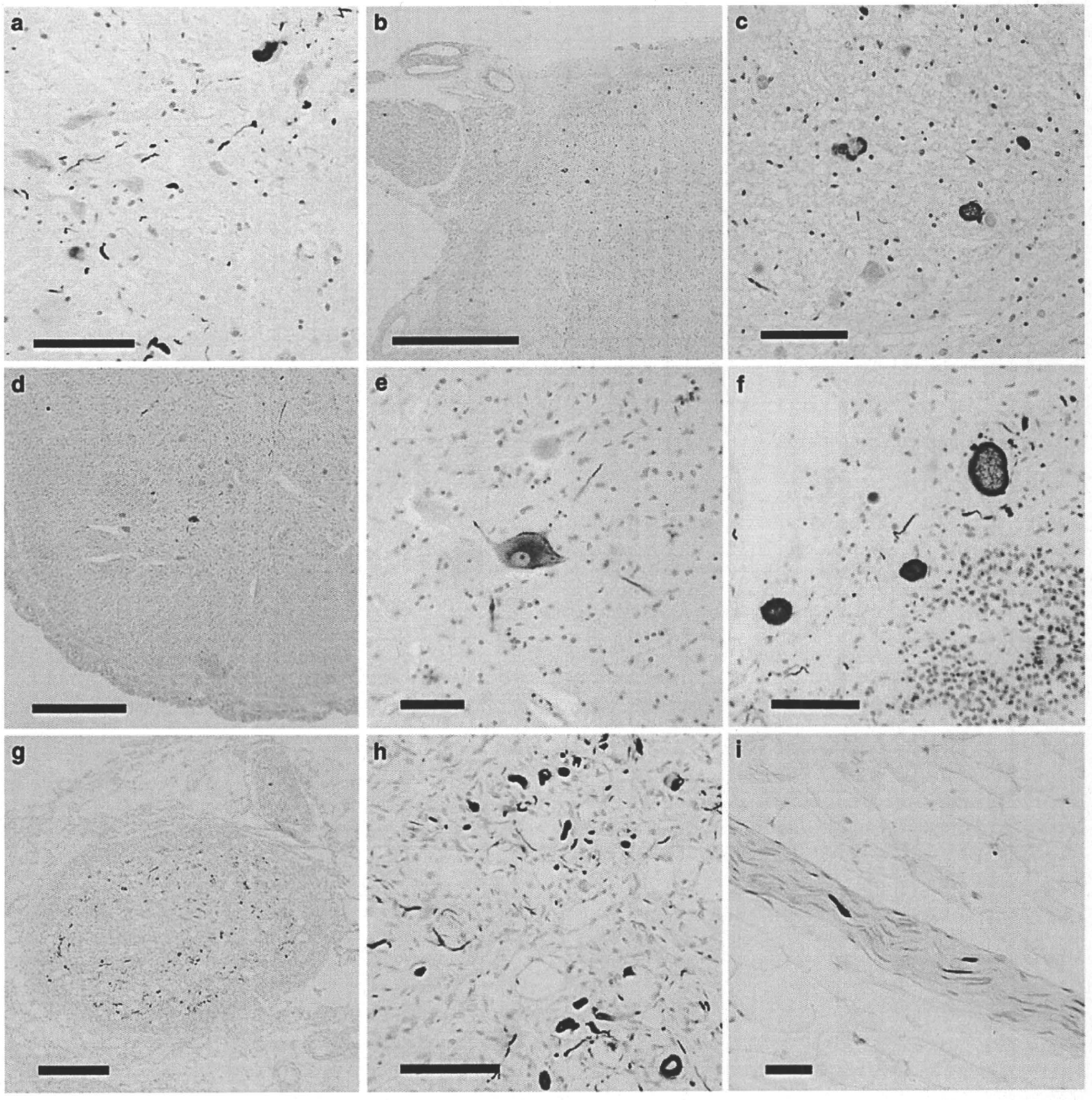


**Fig. 1** Photomicrographs of slides of immunohistochemical staining for phosphorylated α-synuclein histopathology (*PASH*) in paraffin sections of the spinal cord, sympathetic ganglia and vagus nerve. Positive staining is *black*, the counterstain is neutral red. **a** The intermediolateral horn of the thoracic spinal cord of a subject with PD, showing immunoreactive fibers, puncta and perikaryal cytoplasmic inclusions. *Calibration bar* 80 μm. **b**, **c** Low and higher magnification images of the posterior root entry into the sacral spinal cord of a subject with DLB, showing immunoreactive neuronal perikaryal staining. *Calibration bar* in **b** 0.3 mm; in **c** 80 μm. **d**, **e** Low and higher magnification images of the anterior horn of the sacral spinal cord in a subject with PD, showing diffuse cytoplasmic perikaryal immunoreactivity of a large motorneuron. *Calibration bar* in **d** 0.5 mm; in **e** 60 μm. **f** Sacral spinal cord adjacent to the central canal of a subject with PD, showing immunoreactive swollen degenerating neurons or neurites. *Calibration bar* 80 μm. **g**, **h** Low and higher magnification images of a middle cervical sympathetic ganglion of a subject with DLB, showing frequent immunoreactive dystrophic neurites, puncta and neuronal perikaryal cytoplasmic inclusions. *Calibration bar* in **g** 0.1 mm; *calibration bar* in **h** 100 μm. **i** Small branch of the vagus nerve in a subject with PD, showing several immunoreactive nerve fibers. *Calibration bar* 60 μm

No positive staining was observed in the abdominal skin in any of the 14 subjects with DLB or PD. Examination of additional sets of immunostained serial paraffin and 80-μm sections of submandibular gland and esophagus from DLB and PD subjects showed positive staining in 22 of 23 subjects for which the extra sections were stained.

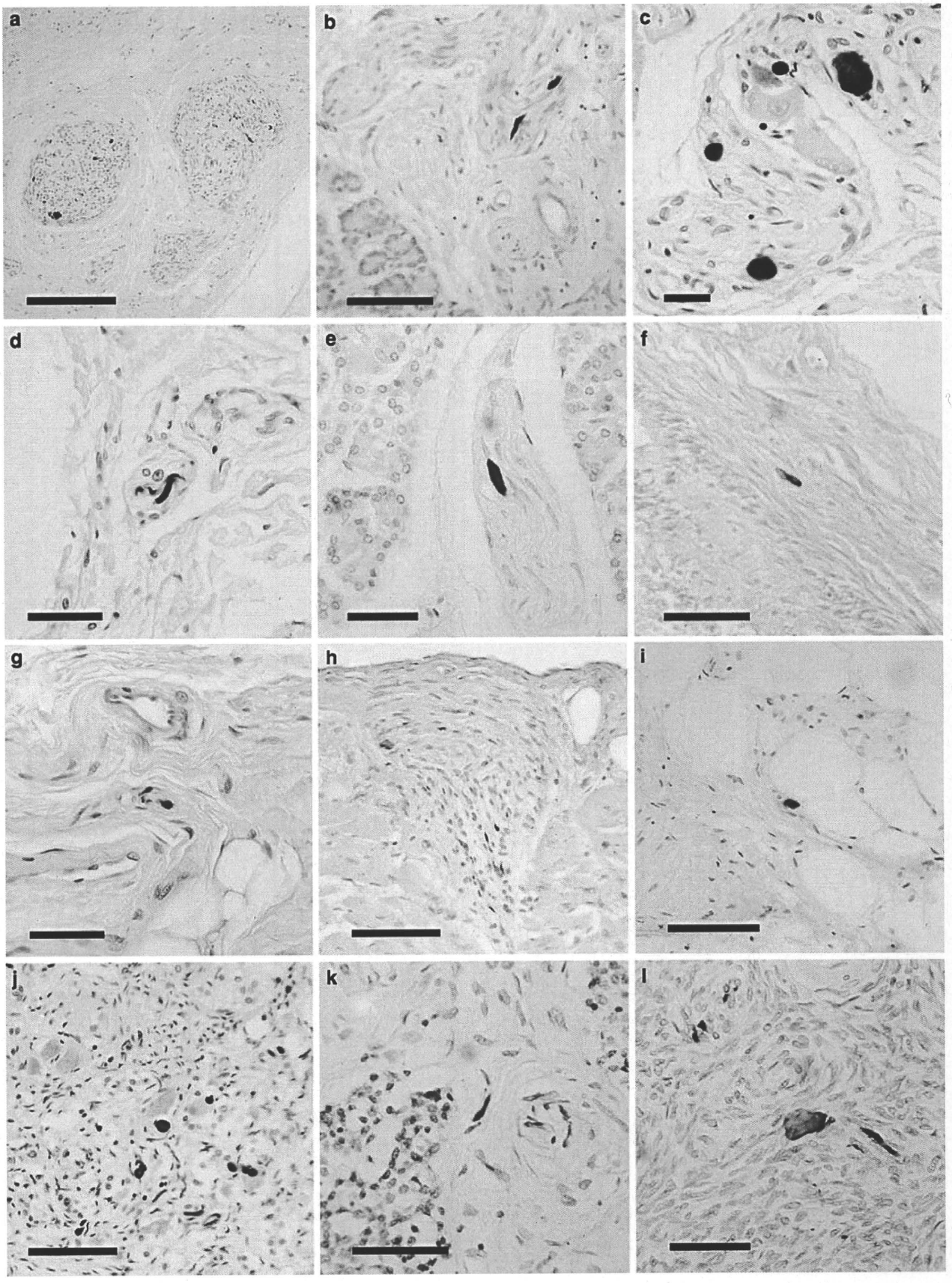
a
b
c
d
e
f
g
h
i
j
k
l